Towards Safe and Personalized Autonomous Driving: Decision-Making and Motion Control with DPF and CDT Techniques

Chao Huang, Chen Lv, *Senior Member, IEEE*, Peng Hang, Yang Xing

***Abstract*—In this paper, a novel approach of decision-making and motion control is designed for realizing safe and personalized driving of autonomous vehicles. A new lane-change intention generation model and a new lane-change decision making algorithm are proposed. The feature of the proposed decision-making module is that the interactions between the ego vehicle and other surrounding vehicles are represented by dynamic potential field (DPF) and embedded in the gap acceptance model to ensure the safety and personalization during driving. In addition, an integrated trajectory planning and tracking control algorithm, which incorporates the artificial potential field (APF) and constrained Delaunay triangulation (CDT) into the model predictive control (MPC) framework, is developed. The newly developed integrated controller allows efficient execution of the expected motion. The proposed approach is tested under different driving conditions and further compared with an existing baseline method. The results show that the proposed approach is able to make safe and personalized decisions, and execute motion control more efficiently for automated driving under dynamic situations, validating its feasibility and effectiveness.**

***Index Terms*—Autonomous vehicles, personalized safe driving, decision making, motion control, DPF, CDT**

I. INTRODUCTION

As a promising mechatronic solution, autonomous driving is expected to help reduce traffic accidents, mitigate human drivers' workloads and further improve the quality and experience of the mobility. However, fully autonomous driving is still far away from mass production and deployment, as currently the smartness of automated vehicles is limited. Thus, the automated vehicle technologies need to be further improved to make reasonable decisions and properly plan motion in various dynamic driving situations, to ensure safety, stability and smoothness. Currently, there are still many open questions and technical challenges existing in the development of automated driving functionality modules, for example, safer and personalized decision making and motion planning, that are worthwhile exploring [1].

For autonomous driving, lane-change (LC) and lane keeping are two important operations that require and assess the ability and performance of decision making and motion planning functionalities [2, 3]. For example, the performance of a lane-change maneuver greatly affects driving safety, ride comfort and traffic efficiency, especially in complex dynamic environments [4]. The study of ref [5] indicates that the lane-change maneuver accounts for about 5% of all crashes and as high as 7% of all crash-related fatalities. Typically, the process of a lane-change maneuver can be divided into two phases: the decision-making and the action execution. The decision-making phase includes the intention generation and lane selection, while the execution phase consists of the generation of a collision-free path and tracking of the generated path.

During a lane-change maneuver, if the current lane cannot meet the controlled vehicle's motion expectation, a lane-change intention will then be generated. To explicitly understand the driver's lane-change intention, a series of surveys is conducted. The study of ref [6, 7] reveals that the velocity difference and distance difference between the ego vehicle and its preceding vehicle mainly affect a driver's lane-change intention generation. Ref [8] suggests that the passenger vehicles commonly change their lanes in order to gain a higher speed. Ref [9] investigates an intention model based on the deceleration to mimic the driver's willingness of lane-change. However, this implicit and indirect expression can not provide an accurate description.

The intention generation is the prerequisite of a lane-change decision-making, and the next step is to assess the safety and feasibility of a lane change manoeuvre and make a decision. The existing methods can be classified as follows: rule-based, discrete models based, game theoretical based and learning-based ones. The principle of the rule-based method is using traffic rules to construct an expert system for traffic gap identification [10]. Some representative rule-based models include the Gipps lane change model [11], CORSIM model [12] and ARTEMiS model [13]. They can be easily implemented in simple scenarios, but would become unreliable in complex driving situations. The main idea of the discrete model is to use an utility function to evaluate the driving gain of each lane and determine the target lane with the maximum gain. However, tuning a large number of weighting parameters would be very time consuming [14]. While Game theory is another typical approach adopted in lane-change decision making. The best maneuver is chosen by maximizing the payoff function [15]. However, the assumptions that each player within the game has the payoff

C. Huang, C. Lv, P. Hang and Y. Xing are with the School of Mechanical and Aerospace Engineering, Nanyang Technological University, 639798, Singapore. (E-mails: {chao.huang, lyuchen, peng.hang, xing.yang}@ntu.edu.sg)
Corresponding author: C. Lv

information of others is not always practical. Recently, learning-based approaches become popular in the lane-change behaviour studies [16]. However, large-size quality data is needed for model training, which causes many restrictions in real world applications. In addition, it does not consider the driver's mental states and cannot make high-level LC decisions that conform to social norms, especially in complex dynamic environments [17].

Through the above review of the lane-change models, it is found that the existing works have not fully considered the driver's aggressiveness level. An aggressive driver may prefer closer cut-ins, closer overtakes, sharper steering operations, etc. And the aggressive driving behaviours may lead to uncomfortable driving experience, improper merging behaviour and higher risks of traffic accidents [18]. A cautious driver, on the contrary, would take care of other surrounding vehicles' intents and benefits. Ref [19] indicate that the aggressiveness level usually correlates to vehicle's longitudinal and the lateral movements. The estimation and classification of the aggressiveness level can be obtained by logic-based methods including constructed driving operational pictures (DOPs) [19], fuzzy logic [20], facial character analysis (FCA)[21], SVM [22], random forest and other learning methods. The logic-based approach is simple and flexible, and can handle problems with imprecise and incomplete data. The learned-based method can improve the estimation accuracy. But, it requires a long time to train models [23].

Once a desirable decision is made, the intended driving maneuver needs to be translated into a trajectory in the target lane [24, 25, 26]. The trajectory planning methods can be categorised as follows: the geometry-based approach [27], optimization-based approach [28] , graph-search approach [29] and Artificial potential field (APF)-based approach [30]. The geometry-based approach is known for its strong ability in calculation efficiency, but it lacks consideration of vehicle dynamics. The optimization-based approach can solve the above drawback, however it may result in a complex non-convex optimization problem which is difficult to be solved. The graph-search approach can generate a cluster of trajectory candidates based on the designed patterns, but it is very time consuming due to a large number of iterations needed. APF is widely used in robotics to navigate an agent to the target place without hitting obstacles. By generating an attractive field attached to the goal point or region and a repulsive field attached to the obstacle, the vehicle motion is then navigated to avoid obstacles. However, the generated route is likely to fall into a local minima due to inappropriate set-up of parameters. To solve it, the combination of APF and model predictive control (MPC) has been developed to provide a continuous and smooth trajectory. But this method is very time consuming.

According to the analysis and comparison conducted above, we aim to develop a novel decision-making and motion control system, which includes a lane-change intention generation model, a decision making model and an integrated trajectory planning and tracking controller. Specifically, the lane-change intention model is firstly developed based on the dynamic potential field and driver's aggressiveness level. Then, a lane-change decision making module is designed using personalized gap acceptance model. Instead of considering the decision-making as a deterministic process, we utilize the conditional probability to build the model for decision-making. Next, an integrated path planning and tracking control module is developed by incorporating CDT and APF into a MPC controller. The contributions of our paper mainly include: 1) a novel personalized lane-change intention model is developed by utilizing DPF and considering the aggressiveness level of driving; 2) a new DPF-based gap acceptance model, which considers both the relative velocity and relative distance, is developed for lane-change decision making to ensure safety and personalization; 3) an new MPC-based motion control algorithm is designed by using CDT and APF to further improve the computation efficiency of the control execution.

The reminder of the paper is as follows. The high-level system structure is introduced in Section II. The decision making method, including the intention estimation of lane-change, estimation of the aggressiveness level, and the safety evaluation of the lane-change maneuver, is introduced in Section III. The path planning and tracking controller are designed in Section IV. The testing, validation and results are presented in Section V. Finally, Section VI concludes this paper.

II. High-Level System Architecture

In order to develop the safe and personalized decision making and motion planning functionalities for autonomous vehicles, a targeted driving scenario is first defined as a straight two-lane motorway, as shown in Fig. 1. For the decision making of the lane change process, we only consider four vehicles, which are the ego vehicle (denoted in short as *ego*) and the preceding vehicle (denoted in short as *preceding*) in the current lane, and the *leader* and *follower* in the target lane.

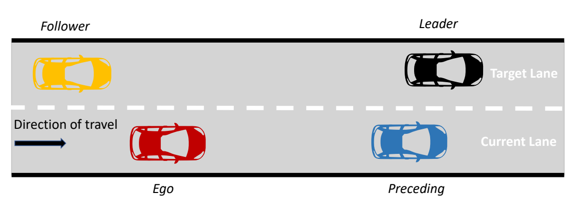

Fig. 1: The defined driving scenario of a two-lane motorway.

The architecture of the entire system to be developed is shown in Fig. 2. By considering the necessity, i.e. the lane-change intention and evaluate the safety, a driving maneuver decision, i.e. either lane-change or lane keeping, will be made. The motion planning and control module will first generate a collision-free corridor by using CDT, and then plan a feasible trajectory by optimizing a constrained multi-objective cost function via the MPC approach.

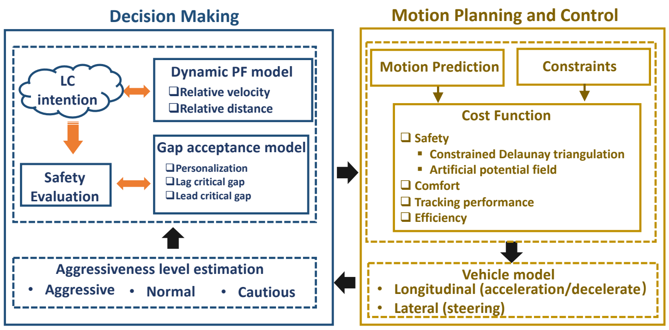

Fig. 2: The high-level framework of the proposed decision-making and motion control approach.

To develop the expected functionalities under the targeted scenario, the following assumptions are made in this work:

- The initial velocity of the *ego* is larger than that of the *preceding*;
- The velocities of the *preceding*, *follower* and *leader* remain constant during the decision making and lane-change process;
- The target lane is the one into which the *ego* is contemplating movement;
- The *ego* is equipped with advanced sensing technology which can provide accurate localization and perception information for executing decision-making;
- During the execution of the lane-change maneuver of the *ego*, the other surrounding vehicles remain in their current lanes [31].

III. The Safe and Personalized Decision-Making

In the decision-making process of a lane-change maneuver, two important factors, namely the necessity and the safety, are considered. The concern of necessity is to determine whether the lane-change maneuver of the *ego* is necessary and the appropriate representation of the personalized intention generation (Section III-A). While the concern on safety is to guarantee a collision-free motion during the lane-change process, and the safety consideration is introduced into a personalized gap acceptance model (Section III-D).

A. Lane-change intention generation

Typically, the ego vehicle executes a lane keeping maneuver when the current lane can meet its expectation. Once the driving expectation cannot be satisfied, for example getting blocked by a slower preceding vehicle, then the lane-change intention is generated. As mentioned in Section I, the willingness of changing the lane mainly depends on the relative distance and relative velocity between the *ego* and *preceding*. Specifically, when the *ego*'s velocity is no larger than that of the *preceding*, the *ego* would prefer to remain in the current lane. When the *ego*'s velocity exceeds that of the *preceding*, the lane-change intention may be generated as their relative distance decreases. In our paper, we adopt the DPF formula to measure the desire of lane-change. As shown in Eq. (1), the DPF model mainly contains two parts: U_Δ and U_{rd}. U_Δ is the von Mises distribution, representing the potential field related to the relative velocity. And U_Δ is the potential field function associated with the relative distance.

$$
\begin{aligned}
U_{pe} &= U_\Delta \cdot U_{rd} \\
U_\Delta &= \alpha \frac{\exp[\eta(\Delta v_{pe})\cos(\theta)] - I}{2\pi I_0[\eta(\Delta v_{pe})]} \\
U_{rd} &= A_f \cdot \exp\left[- \left[\frac{(x_e - x_p)^2}{2\sigma_x^2} + \frac{(y_e - y_p)^2}{2\sigma_y^2} \right]^b \right]
\end{aligned} \tag{1}
$$

where α is the maximum value of the potential field of U_Δ. A_f is the maximum value of the potential field of U_{rd}. θ is the relative heading angle between the two vehicles. $\Delta v_{pe} = v_p - v_e$ is the relative velocity, and v_e is the *ego*'s velocity and v_p is the *preceding*'s velocity. $(x_i, y_i), i \in \{e, p\}$ represents the *ego*'s position and *preceding*'s position, respectively. σ_x and σ_y stand for the convergence coefficients along the directions of axis X and Y, respectively. b is the coefficient for changing the shape. $I_0(\cdot)$ is the modified Bessel function of 0 order. By using U_Δ, the potential field is drifted to the direction of Δv. It should be noted that the distributions of the potential field in vehicle's longitudinal and lateral directions are different. In our study, we set $\eta(\Delta v_{pe}) = a\,\mathrm{sign}(\Delta v_{pe})|\Delta v_{pe}|$ where a is a design parameter.

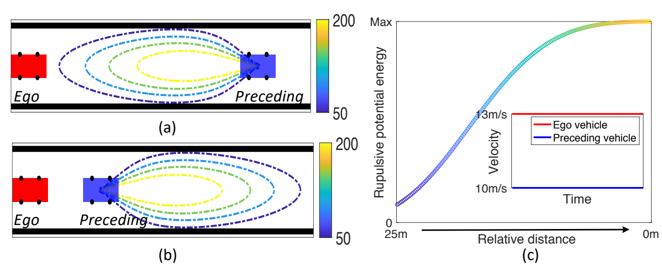

Fig. 3: Schematic diagram of the dynamic potential field designed based on the relative velocity and distance: (a) the distribution of the DPF when *ego* is faster than *preceding*; (b) the distribution of the DPF when *ego* is lower than *preceding*; (c) dynamic potential field with $v_e = 13m/s$ and $v_p = 10m/s$.

As shown in Fig. 3, if the *ego* moves faster than the *preceding*, the drifted potential field will be generated towards the *ego* (Fig. 3a). While the distribution of the potential field will be drifted forward if the *ego* is slower than the *preceding* (Fig. 3b). Additionally, Fig. 3c shows the relationship between the potential field and the relative distance. It shows that with the decrease of the relative distance, the repulsive potential field is

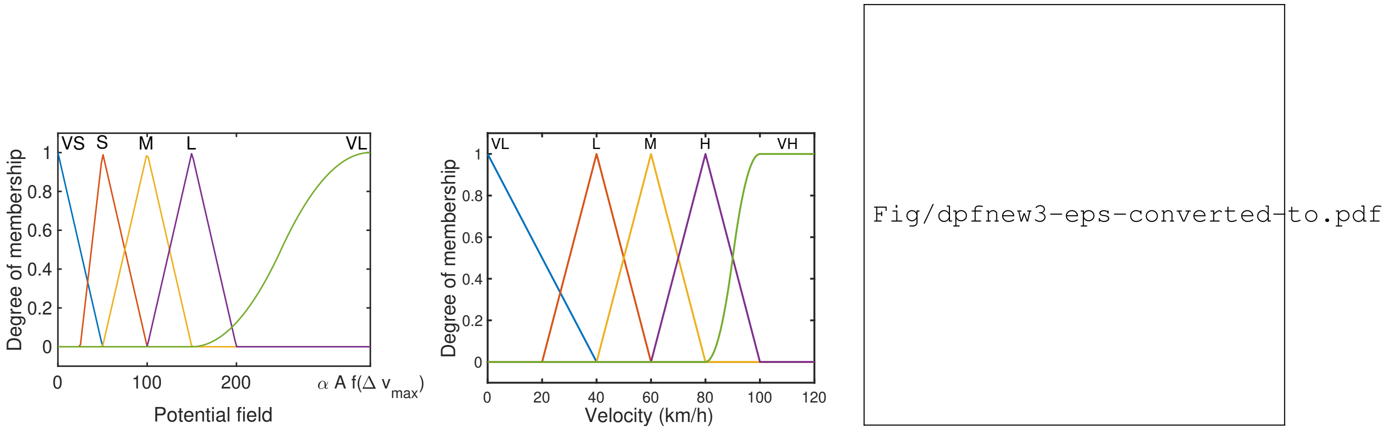

(a) (b) (c)

Fig. 4: The membership functions: (a) the potential field; (b) vehicle's velocity; (c) the aggressiveness level.

increased and reaches its peak value when the relative distance converges to zero. Based on this relation, if the *ego* cruises at a velocity that is no larger than the *preceding* and there's no braking operation executed, then it will be considered as beyond a relatively safe distance.

As there are considerable interpersonal differences in driver's decision-making and driving performance, it is reasonable to consider driver's personalization. To realize personalized safe driving, it is necessary to select different values for the threshold of the lane-change intention generation module. Once the intention is triggered, the larger the potential energy is, the stronger the lane-change intention will be. Vice versa. To do this, a concept of aggressiveness level is introduced in this work for representing the personalization, and it will be associated with the threshold selection of the lane-change intention generation.

B. Estimation of the aggressiveness level

In this work, the aggressiveness level of the *ego*'s driving is estimated to indicate the willingness of the lane-change maneuver and therefore to determine the threshold of lane-change intention. Here, we divide the aggressiveness levels into the following groups:

- Type A: low aggressiveness, i.e. cautious driving. The drivers care about their safety and surrounding vehicle's benefits. Thus, they prefer to stay in the current lanes, maintaining within a relatively safe condition.
- Type B: medium aggressiveness, i.e. normal driving. This driving style is positioned in between the aggressiveness and cautious ones. The drivers prefer to do lane changes when risks are low.
- Type C: high aggressiveness, i.e. aggressive driving. The drivers would like to take some risks to reach their driving objectives (including higher speed and shorter travelling time) whenever they have a chance.

Remark 3.1: The repulsive potential energy is inversely proportional to the relative distance under a fixed relative velocity, and the average potential energy is usually calculated over a period of time. However, in this work, under the assumption that the vehicles remain their velocities during a lane change maneuver, we are able to use the *ego*'s initial velocity and initial potential energy as the factors to determine the aggressiveness level.

In order to classify the aggressiveness level, the Fuzzy inference system (FIS) approach is adopted in this study. FIS is utilized for mapping the inputs with the outputs by using the fuzzy membership functions and fuzzy rules. This method has been widely used in many application domains [32]. It consists of three main components: the fuzzification, the rule evaluation and the defuzzification. With FIS, the aggressiveness level of driving can be estimated as:

1) Fuzzification: Fuzzification is a process to convert a input value to a fuzzy value based on the membership functions. In this work, the triangular membership functions and S-shaped membership function are utilized. The fuzzy values of potential field applied are listed as follows: very small (VS), small (S), medium (M), large (L) and very large (VL). The fuzzy values of vehicle's velocity can be defined as: very low (VL), low (L), Medium (M), High (H) and very high (VH). The output is the level of the driving aggressiveness: low (L), medium (M) and high (H). The membership functions are shown in Fig. 4.

2) Rule evaluation: The fuzzy rules are used to describe how the FIS system makes a classification regarding the inputs. In thsi work, the fuzzy rules are represented in the form of *If-and-Then* and are summarized in TABLE I.

3) Defuzzification: Defuzzification is the process that computes the output values based on the membership function. There are many methods, including center of area (COA), mean of maximums (MEMAX), center of gravity (COG) and weighted mean of maximums (WMEMAX), for solving the defuzzification. In thsi work, the COG approach is adopted to estimate the level of the aggressiveness of *ego* which is parameterized by $\rho_e, 0 \leq \rho_e \leq 1$. The greater the value of

TABLE I: Fuzzy rules for aggressiveness level identification

Index	Potential field	Operator	Velocity	Rule weight	Output
1	VS	and	VL	1	L
2	VS	and	L	1	L
3	VS	and	M	1	M
4	VS	and	H	1	M
5	VS	and	VH	1	M
6	S	and	VL	1	L
7	S	and	L	1	M
8	S	and	M	1	M
9	S	and	H	1	M
10	S	and	VH	1	H
11	M	and	L	1	M
12	M	and	M	1	M
13	M	and	H	1	M
14	M	and	VH	1	H
15	L	and	L	1	M
16	L	and	H	1	H
17	L	and	VH	1	H
18	VL	and	L	1	H
19	VL	and	H	1	H
20	VL	and	VH	1	H

the ρ_e is, the more aggressive the *ego* is.

C. Personalized decision making model

Based on the estimation of aggressiveness level of driving, the personalized decision making model is developed. Different thresholds in the relative distance-relative velocity state plane as is designed for different driving styles as shown in Fig. 5. The lane-change intention is considered to be triggered by different reference thresholds under different aggressiveness levels of the *ego*, which can be reflected in the potential field. Suppose that the initial point of the relative velocity and initial relative distance between the *ego* and *preceding* is represented by A. As the relative velocity is assumed to be constant during the lane-change process, their relative distance will gradually decrease over time, as shown by the vertical black dash line downwards. After the relative distance reaches the threshold line of intention generation (Point B), the *ego* starts to plan a lane change. Based on our previous definition, the vehicles of a high aggressiveness would generate the lane-change intention much earlier than those ones with medium and low aggressiveness (normal and cautious). Thus, the corresponding threshold line for the intention generation of aggressive ones would be closer to the initial point, as reflected in the figure.

The point S in Fig. 5 shows an emergency situation after which the *ego* has to slow down at its maximum deceleration in order to avoid the potential rear-on collision to the *preceding*. The calculation of the minimal safe distance can be given by:

$$d_s = \frac{v_e^2 - v_p^2}{2a_{max}} + v_e(t_r + \frac{t_i}{2}) + d_o \tag{2}$$

where t_r is the reaction time ranging from $0.8s$ to $1s$ for human driving. In this work, it is set as $0.1s$ for the faster responsiveness of autonomous vehicle. t_i is the build-up time of deceleration ranging from $0.1s$ to $0.2s$. a_{max} is the maximum

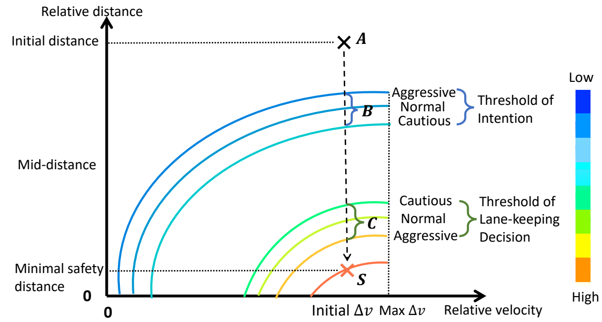

Fig. 5: Schematic diagram of the reference line for decision making.

deceleration for both the *ego* and *preceding*. d_o is the minimum clearance distance between the adjacent vehicle after the *ego* reaches the same velocity as the *preceding*, and set d_o as $2m$ in this work. Point S is the point we would like to avoid. Therefore, the threshold line for lane keeping (Point C) is designed to be above the Point S. Point C represents the threshold for the lane keeping decision generation. We assume that if a safe lane-change decision is confirmed when the current state point is within the segment BC, then a lane-change maneuver will be executed immediately. Otherwise, a lane keeping decision will be made once the *ego* reaches the Point C.

For simplification, the lateral positions of the *ego* and *preceding* are the same, i.e., $y_e = y_p$. Then (1) can be rewritten in a more general form as:

$$U(\Delta v_{pe}, d_{pe}) = A\frac{\exp[\eta(\Delta v)\cos(\pi)] - I}{2\pi I_0[\eta(\Delta v)]}\exp\left[-\left[\frac{d_{pe}^2}{2\sigma_x^2}\right]^b\right] \tag{3}$$

where $A = \alpha \cdot A_f$ and $d_{pe} = x_e - x_p$ is the relative distance between *ego* and the *preceding* in the longitudinal direction. It can be seen that $U_{(\cdot)}$ is a function of the relative velocity and relative distance. Then, the threshold line of the potential field for lane-change intention can be calculated as

$$U_B = U\left(\Delta v_{el}, \left[d_{pe0} - \left|\frac{\exp(\beta_i(1-\rho_e))}{e}\right|\left[\frac{d_{pe0} - d_s}{2}\right]\right]\right) \tag{4}$$

where d_{pe0} is the initial relative distance. β_i is a coefficient. ρ_e is the estimated aggressiveness level of *ego*. Δv_{el} is the relative velocity between the *ego* and the *leader* ($\Delta v_{el} = v_e - v_l$).

Similarly, the potential field of the threshold line for lane keeping is designed as

$$U_C = U\left(\Delta v_{ef}, \left[\frac{d_{pe0} + d_s}{2} - \left|\frac{\exp(\beta_i \rho_e)}{e}\right|\left[\frac{d_{pe0} - d_s}{2}\right]\right]\right) \tag{5}$$

where Δv_{ef} is the relative velocity between the *ego* and the *follower* ($\Delta v_{ef} = v_e - v_f$).

As discussed above, a suitable decision can be made before the *ego* entering the emergency region. It should be noted that position of Point B, C and S may move up or down in parallel due to the external disturbance or measurement error. After a lane-change intention is generated, the safety of during the possible lane-change maneuver will be evaluated for the *follower* and *leader*.

D. Safety evaluation of the the lane-change maneuver

In order to evaluate vehicle's safety during a lane-change maneuver, in this work, the concept of critical gap is used. The critical gap consists of lead critical gap and lag critical gap [33]. The lane-change maneuver is considered as safe and feasible only when both the lead and lag critical gaps are acceptable (Fig. 6). The lead and lag critical gaps are selected based on the relative velocity between the *leader* and the *follower*, and they can be calculated as:

$$\begin{aligned} G_l &= \exp(\eta_l + \kappa_l U(\Delta v_{el}, d_{el}) + \beta_l(1-\rho_e)) \\ G_f &= \exp(\eta_f + \kappa_f U(\Delta v_{fe}, d_{ef}) + \beta_f(1-\rho_e)) \end{aligned} \tag{6}$$

where $U(\Delta v_{ij}, d_{ij}), i, j \in \{e, f, l\}$ represents the potential energy and can be calculated through Eq. (3). $v_{ij} = v_i - v_j$ and d_{ij} denote the relative velocity, and the relative distance between vehicle i and vehicle j, respectively. η_i, κ_i and $\beta_i, (i = l, f)$ are design parameters. It should be noted that only when both G_l and G_f are smaller than the corresponding real gaps, then the lane-change maneuver will be considered as safe and executable.

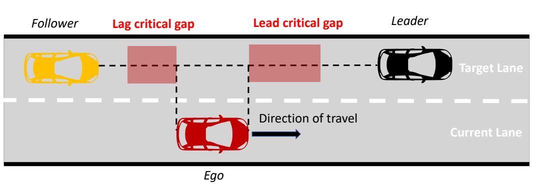

Fig. 6: The gap acceptance model for the LC decision making.

As described in Eq.(6), the lane-change decision is made based on the aggressiveness level of the *ego* and the potential field forces generated by the *leader* and the *follower*. When the *ego* moves faster than the *leader*, as their relative distance decreases, the lead critical gap needed by the *ego* for doing a safe lane-change would become larger. Similarly, the lag critical gap increases as the relative velocity between the *follower* and the *ego* increases. In addition, by introducing ρ_e to Eq.(6), the calculated gap can match with the human driver's characteristics. As described in Eq. (6), a larger gap is needed for an autonomous vehicle with a lower aggressiveness than that for one with a higher aggressiveness. The probability for executing a lane change is therefore given by

$$\begin{aligned} &P(\text{LC}) \\ &= P[G_l^{real}(t) > G_l(t)|\rho_e] \cdot P[G_f^{real}(t) > G_f(t)|\rho_e] \end{aligned} \tag{7}$$

where G_l^{real} and G_f^{real} are the real lead gap and real lag gap, respectively. The conditional probabilities that the lead and lag gaps are acceptable can be derived as

$$\begin{aligned} &P[G_l^{real}(t) > G_l(t)|\rho_e] \\ &\quad = P(\ln(G_l^{real}) > \ln(G_l)|\rho_e) \\ &\quad = \Phi\left(\frac{\ln(G_l^{real}) - \ln(G_l)}{\sigma_l}\right) \end{aligned} \tag{8}$$

and

$$\begin{aligned} &P[G_f^{real}(t) > G_l(t)|\rho_e] \\ &\quad = P(\ln(G_f^{real}) > \ln(G_f)|\rho_e) \\ &\quad = \Phi\left(\frac{\ln(G_f^{real}) - \ln(G_f)}{\sigma_f}\right) \end{aligned} \tag{9}$$

where $\Phi(\cdot)$ is the cumulative standard normal distribution, σ_l and σ_f denote the variance of the lead gap and the lag gap, respectively. If $P(\text{LC}) > 1 - P(\text{LC})$, a lane-change decision will be made.

IV. Safe and Efficient Motion Planning and Tracking Control

In this section, we formulate the path planning and tracking control problem together as an integrated module. Firstly CDT technique is used to identify the safe area from the current position of the *ego* to the target point based on the driving decision made (Section IV-A). The boundary of the safe area is then represented by the APF model (Section IV-B). Then, a CDT-APF based MPC controller is designed to simultaneously plan the local path and optimize the control outputs (i.e. the front wheel steering angle and the longitudinal acceleration) in real time (Section IV-C). It should be noted that the artificial potential field in this section is different from the one, i.e the dynamic potential field model, used in Section III.

A. Collision-free driving area

In this work, CDT is adopted to determine the safe area for generating collision-free paths. The Delaunay triangulation graph can dynamically updated based on the changes occurred in the dynamic driving environment. The target region is defined as the position that is away from the *leader* or *preceding* with a distance of d_o. The safe area consists of a sequence of triangles which connects the starting point to the final region (Fig. 7).

The method for identifying the safe area can be summarized as follows:

(1) After a decision is made, identify the target region and regard all the surrounding vehicles as rectangle obstacles;

(2) Discrete the driving region into N constrained Delaunay triangles. Find the triangle $T_s, T_f \in \mathcal{T}, 1 \le s, f \le N, f \neq s, \mathcal{T} = \{T_1, T_2, \cdots, T_N\}$ to which the starting point S_p and final point F_p belong.

(3) Construct an adjacent matrix $\mathbf{M}^{N\times N}$ to indicate the adjacency of any pair of the triangles. The element $\mathbf{M}(j, m) =$

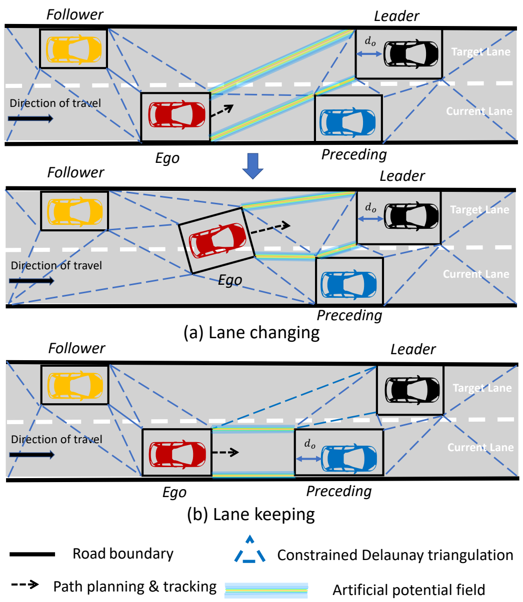

Fig. 7: The path planning scheme with CDT and APF.

$1, (j = 1, \cdots, N, m = 1, \cdots, N)$ when the triangles T_j and T_m are adjacent. Otherwise, $\mathbf{M}(j, m) = 0$.

(4) Based on the adjacent matrix $\mathbf{M}$, create a tree structure to find a possible way from T_s to T_f through a sequence of triangles. The tree construction can be summarised in **Algorithm** 1. In **Algorithm** 1, τ is a tree structure whose root is T_s. **InsertTree**() is used to insert a node to the current tree under the father node $farnode$, while $branch$ is a sequence of nodes from root to the leaf node. After the safe area is identified, the boundary of the safe area is then considered as non-overcome road boundary and can be represented through the APF model.

Algorithm 1 Tree construction

Inputs : Triangles T_s, T_f
Adjacent matrix $\mathbf{M}$
Output: τ
Initialize: $\tau \leftarrow$ **InitializeTree**(T_s),
Set **Searchentity**$= \{T_s\}$
while ***SearchEntity***$\neq \emptyset$ **do**
  $farnode$=**SearchEntity**(1)
  SearchEntity=SearchEntity-$\{farnode\}$
  SearchEntity= SearchEntity $\cup \mathbf{M}(farnode, :)$
  $Index = find(\mathbf{M}(\text{farnode}, :) == 1)$
  for $i = 1 : 1 : length(Index)$ **do**
    $childnode = T_{Index(i)}$
    $[\tau,\ addnum] \leftarrow$ **InsertTree** $(\tau, farnode, T_{Index(i)})$
    if $childnode \neq T_f$ & $addnum \geq 1$ & $childnode \notin$ ***SearchEntity*** **then**
      SearchEntity $\leftarrow$ **SearchEntity** $\bigcup\{childnode\}$
    end
  end
end

B. Artificial potential field model

In this section, we assign repelling artificial potential fields to the boundary of the safe area:

$$P^r(x, y) = e^{(-r_i + d_c + \frac{w}{2})\cdot h} \tag{10}$$

where $r_i, i = \{low, up\}$ represents the minimum distance from the point (x, y) to the *lower* boundary and the *upper* boundary of the safe area. w is the vehicle width and d_c is the safety margin. h is the coefficient to adjust the magnitude of the potential field value. The value of $P^r(x, y)$ should be large enough to keep the *ego* within the safe area.

C. Model predictive controller design

In this section, we design a CDT-APF based MPC controller for path planning and tracking control. A dynamic vehicle model with three degrees of freedom is adopted. The state variables are $x = [x^{\oplus}, y^{\oplus}, \psi, v_x, v_y, r]$. $(x^{\oplus}, y^{\oplus})$ are the longitudinal and lateral positions, respectively, in the body frame (X, Y). v_x and v_y denote the longitudinal and lateral speeds of the centre of mass (CM), respectively. $r = \dot{\psi}$ is the yaw rate and ψ is the inertial heading angle. The dynamics of the vehicle can be modeled as follows [34]:

$$\begin{aligned} \dot{v}_x &= r v_y + a_x, \\ \dot{v}_y &= -r v_x + \frac{2}{m}(F_{cf}\cos\delta_f + F_{cr}), \\ \dot{r} &= \frac{2}{I_z}(l_f F_{cf} - l_r F_{cr}), \\ \dot{x}^{\oplus} &= v_x \cos\psi - v_y \sin\psi, \\ \dot{y}^{\oplus} &= v_x \sin\psi + v_y \cos\psi. \end{aligned} \tag{11}$$

where m and I_z denote the vehicle's mass and yaw inertia, respectively. a_x is the longitudinal acceleration, and δ_f is the steering angle of the front wheel. l_f and l_r represent the distances from the CM of the vehicle to the front and rear axles, respectively. R_w is the rolling radius. F_{cf} and F_{cr} denote the lateral tyre forces at the front and rear wheels, respectively. Tthe systems' input is $u = [\delta_a\ a_x]^T$. We discretize the vehicle system with a fixed sampling time T_p and obtain $x_{k+1} = f^d(x_k, u_k)$ and $y_k = P^r(x_k^{\oplus}, y_k^{\oplus})$. y_k is the potential field value associated with the position coordinates. Then, the optimization problem can be formulated as:

$$\begin{aligned} \min_{\mathcal{U}_t, \epsilon} \sum_{k=1}^{H_p} \|y_{t+k,t}\|_R^2 + \|y_{t+k,t}^{\oplus} - y_{target}\|_W^2 + \|v_{t+k,t} - v_{target}\|_H^2 \\ + \|\frac{dr_{t+k}}{dt}\|_N^2 + \sum_{k=1}^{H_c} \|u_{t+k,t}\|_Q^2 \end{aligned} \tag{12}$$

$$s.t.\ x_{t+k+1,t} = f^d(x_{t+k,t}, u_{t+k,t}),\ k = 0, \cdots, H_p - 1 \quad (13a)$$
$$y_{t+k,t} = \left[y_{k+1,t}, \cdots, y_{k+H_p,k}\right]^T \quad (13b)$$
$$u_{t+k,t} = \Delta u_{t+k,t} + u_{t+k-1,t} \quad (13c)$$
$$u_{min} \leq u_{t+k,t} \leq u_{max},\ k = 0, \cdots, H_c - 1 \quad (13d)$$
$$u_{t-1,t} = u(t-1) \quad (13e)$$
$$x_{t,t} = x(t) \quad (13f)$$

where t denotes the current time, and $x_{t+k,t}$ denotes the predicted state at time $t+k$ obtained by applying control sequence $\mathcal{U}_t = [u_{t,t}, \cdots, u_{t+k,t}]$ to the system $(x_{k+1} = f^d(x_k, u_k))$ with $x_{t,t} = x(t)$. R, W, H and N are the output weighting matrices, and Q is the weighting factor of the control input. H_c is the control horizon, while H_p is the prediction horizon with $H_p \geq H_c$. The first term is the core of the CDT-APF-based MPC controller. It aims to minimize the potential energy given by APF model. In this way, the position of *ego* is constrained in a relatively narrow space, i.e., safe area, so that the *ego* can quickly move to the target lane under the repulsive force. The second and the third terms aim to make the *ego* drive consistently with the *target* in the lateral direction and reduce their relative speed. The *target* vehicle is either the *leader* or the *preceding* vehicle. The forth term aims to minimize the yaw acceleration throughout the maneuver, ensuring driving comfort and efficiency. The final term reflects the consideration on the size of $u_{t+k,t}$. The control inputs are $u = \left[\delta_f, a_x\right]$, and they both subject to the physical limitations of the vehicles, i.e., $\delta_{fmin} \leq \delta_f \leq \delta_{fmax}$ and $a_{xmin} \leq a_x \leq a_{xmax}$. δ_{fmin}, δ_{fmax}, a_{xmin} and a_{xmax} denote the saturation level of δ_f and a_x, respectively. The above optimization problem can be effectively solved by using the *fmincon* in MATLAB environment. It should be noted that the above optimization problem can be transferred to a Min-Max MPC optimization problem when considering measurement error and disturbance.

V. Testing, Validation and Results

In this section, the proposed approach will be tested in autonomous vehicles under typical scenarios, and its feasibility and effectiveness will be validated. Results will be reported and discussed.

A. Testing scenario

The testing scenario is set as follows:

1) The driving scenario is the two-lane motorway, and the road width is set as 3.5m.
2) The *ego* vehicle starts from the initial position at $(0, 0)$.
3) The physical limitations on vehicle actions are set as $-30 \times \frac{\pi}{180} \leq \delta_f \leq 30 \times \frac{\pi}{180}$ and $-5 \leq a_x \leq 5$.
4) The sampling time is set as $0.05s$. The control horizon is $H_c = 5$, while the prediction horizon is $H_p = 10$.
5) Other initial setting of the driving scenario is listed in TABLE II.

TABLE II: Environment set-up in the testing

Parameter	Value
Initial velocity of the *ego*	13 m/s, 15 m/s and 9 m/s
Initial velocity of the *preceding*	10 m/s
Initial distance to the *preceding*	35 m
Initial velocity of the *leader*	14 m/s
Initial velocity of the *follower*	12 m/s
Initial distance to the *leader*	5 m
Initial distance to the *follower*	20 m

6) The parameters of the *ego*, the dynamic potential field used in Section III-A and the gap acceptance model used in Section III-D are selected as the same as ones in [33].

B. Testing results

Based on the above different settings of the driving environments, the corresponding probabilities of aggressiveness can be calculated, representing the medium, high and low levels of the aggressiveness, respectively:

$$\rho_e = 0.5139,\ v_{e0} = 13\ [m/s],$$
$$\rho_e = 0.7163,\ v_{e0} = 15\ [m/s],$$
$$\rho_e = 0.2969,\ v_{e0} = 9\ [m/s].$$

Fig. 8 shows the results of decision making and motion control with $\rho_e = 0.5139$. Fig. 8a shows a lane-change trajectory of the *ego* by considering it own driving aggressiveness and surrounding vehicles. Fig. 8b-d represent the *ego*'s status at three different time points during the execution of a planned lane change. It shows that at each time step, the current driving maneuver can be discretized into several constrained Delaunay triangles, which are indicated by the dash blue line. The safe area that the *ego* travels is identified, and the information of the corresponding boundary (the solid purple line) is implemented in the potential field model. The proposed controller can generate a collision-free and smooth path for lane-change of the *ego*.

To analyze the impact of aggressiveness level on the decision making process, Fig. 9 , which represents the vehicle's status under different aggressiveness levels, is plotted. Subfigs. 9a-c illustrate the time point of lane change intention generation, lane change decision-making and lane departure with different aggressiveness levels, respectively. For example, in Fig. 9a, the lane-change intention is generated when the *ego* reaches around $35m$ in the longitudinal direction. The safety evaluation of the lane-change maneuver is updated in real time, and a safe lane-change is confirmed as reflected by the flag in $LC_{safety} = 1$. After the *ego* moves cross the dashed lane line and further moves towards the target lane, there is no more lane-change intention generated, as the flag changes back to 0 $LC_{intention} = 0$. In addition, as shown in Fig. 9b, a more aggressive *ego* vehicle generates the lane-change intention earlier and executes the maneuver quickly since the limitations on its acceptable gap is relative loose. In contrast, a cautious *ego* vehicle, as shown in the Fig. 9c, is more likely to make a conservative decision, as it only

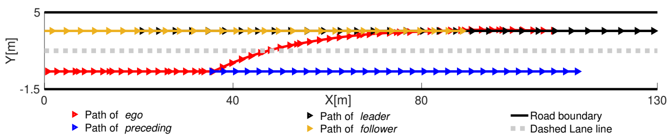

(a) Results of vehicles' paths during the lane-change maneuver

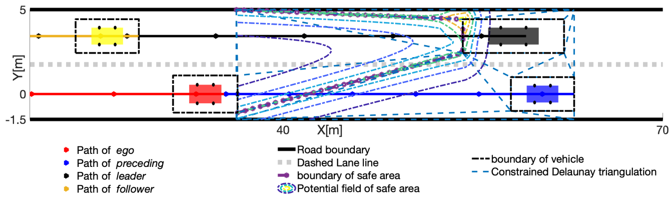

(b) Results during the lane-change maneuver at t=2.8s

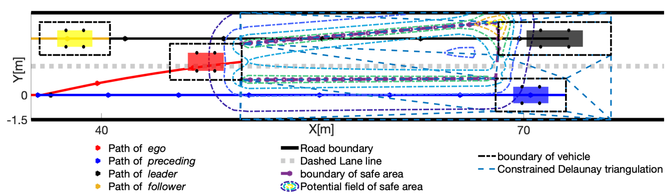

(c) Results during the lane-change maneuver at t=3s

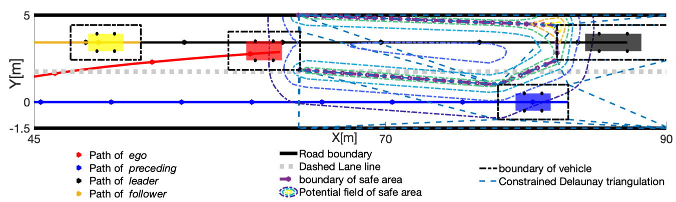

(d) Results during the lane-change maneuver at t=3.3s

Fig. 8: Results of the decision making during the lane change under the medium level of aggressiveness ($\rho_e = 0.5139$).

performs the lane-change maneuver when the gap is relative large. This conservative behaviour then leads to a lane keeping decision ($LK_{safety} = 1$). Fig. 9d shows the velocity tracking performance under different aggressiveness settings. This is the third objective of the optimization problem and can be achieved by controlling a_x.

Discussion: The testing results show that the proposed approach is able to represent autonomous vehicles' various driving patterns by considering different aggressiveness levels during the decision making process. Meanwhile, by implementing the DPF in the gap acceptance model, the interactions between the *ego* and its surrounding vehicles can be well represented, and the safety and feasibility of the lane-change maneuver can be effectively evaluated.

Remark 5.1: It can be inferred that the proposed approach can work well in complex multi-lane scenarios as long as the *preceding* in the current lane and *follower* and *leader* in target lane can be accurately identified.

Besides the above testing of the decision-making functionality, the effectiveness and superiority of the proposed motion controller also need to be validated. In this work, it is tested and compared with a typical existing baseline method, i.e. the APF-MPC based method. APF-MPC method has been widely studied and used for collaborative driving and path planning [35]. We compare the proposed approach with the APF-MPC method with respect to the response time of decision-making and trajectory planning performance. As the APF-MPC based method incorporates the artificial potential filed model into a MPC controller, thus, for comparison, the repulsive potential field model is designed as same as the one in (10). And the attractive potential field model is based on the velocity difference between the *ego* and the target vehicle (the *leader* or the *preceding*).

The comparison results of the path planning and tracking control during the lane-change maneuver are shown in Fig. 10. The Fig. 10 shows that both approaches can provide a collision-free trajectory for the lane change maneuver. However, the proposed one (the red line) is able to provide a faster response to the decision made, and therefore the *ego* would move faster to the target lane. The reason for this phenomenon is that the repulsive force generated based on CDT in the proposed method can provide a more explicit guidance during path planning as shown in Fig. 10c. In contrast, the repulsive force generated by the APF-MPC method is not concentrated nor large (Fig. 10b). Therefore, the *ego* cannot quickly execute a lane change maneuver under the baseline method. Fig. 10d also indicates that the proposed approach can effectively improve the yaw motion, ensuring the vehicle's stability during the lane change process. These testing results validate that the proposed motion control algorithm is able to effectively execute the personalized decision-making and plan safe trajectories, showing its advantages over the conventional method.

VI. Conclusion

This paper investigates the safe and personalized decision making and motion planning approach for autonomous driving. A DPF-based model is firstly designed to describe the intention generation of lane-change maneuvers for autonomous vehicles. Then the gap acceptance model is developed to evaluate the safety of the lane-change process by considering the interactions between the *ego* vehicle and surrounding ones. Next, an integrated path planning and tracking control algorithm is developed to effectively execute the motion controls using combined CDT and APF techniques.The simulation results show that the proposed approach is able to make safe and personalized decisions, and execute the motion control more efficiently for automated driving under dynamic situations, validating the its feasibility and effectiveness. Our further work will focus on the algorithm improvement with consideration of measurement error and disturbance, as well as the evaluation of the proposed approach on an real-time experimental platform.

Acknowledgment

This work was supported in part by the SUG-NAP Grant (No. M4082268.050) of Nanyang Technological University,

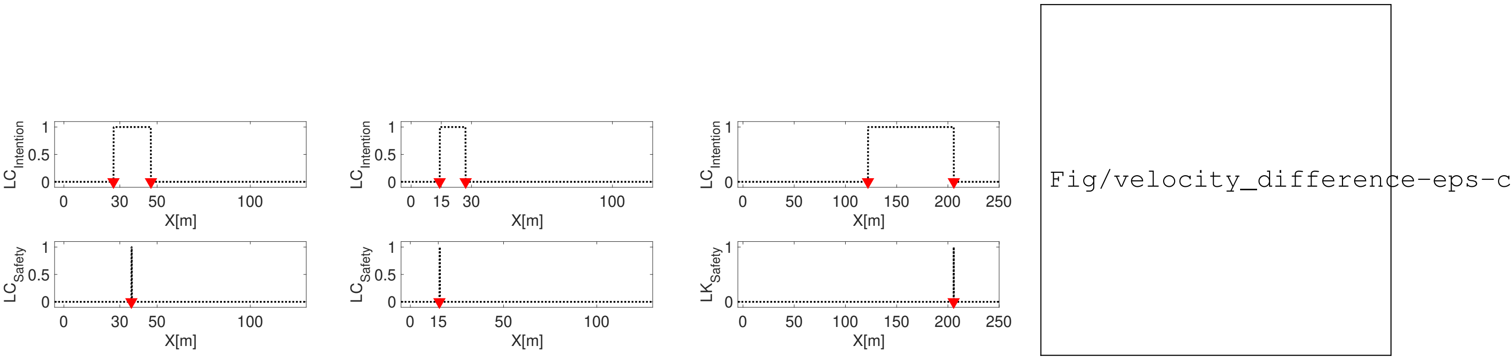

(a) Results of $\rho_e = 0.5139$ (b) Results of $\rho_e = 0.7163$ (c) Results of $\rho_e = 0.2969$ (d) Velocity difference

Fig. 9: Results of the decision making process under different aggressiveness levels.

Singapore, and A*STAR Grant (No. 1922500046), Singapore.

References

[1] X. Li, Z. Sun, D. Cao, Z. He, and Q. Zhu, "Real-time trajectory planning for autonomous urban driving: Framework, algorithms, and verifications," *IEEE/ASME Transactions on Mechatronics*, vol. 21, no. 2, pp. 740–753, 2015.

[2] Y. Zhang and P. A. Ioannou, "Combined variable speed limit and lane change control for highway traffic," *IEEE Transactions on Intelligent Transportation Systems*, vol. 18, no. 7, pp. 1812–1823, 2016.

[3] H. Yoshida, S. Shinohara, and M. Nagai, "Lane change steering manoeuvre using model predictive control theory," *Vehicle System Dynamics*, vol. 46, no. S1, pp. 669–681, 2008.

[4] Z. Wang, G. Li, H. Jiang, Q. Chen, and H. Zhang, "Collision-free navigation of autonomous vehicles using convex quadratic programming-based model predictive control," *IEEE/ASME Transactions on Mechatronics*, vol. 23, no. 3, pp. 1103–1113, 2018.

[5] Y. Hou, P. Edara, and C. Sun, "Situation assessment and decision making for lane change assistance using ensemble learning methods," *Expert Systems with Applications*, vol. 42, no. 8, pp. 3875–3882, 2015.

[6] P. Hidas, "Modelling vehicle interactions in microscopic simulation of merging and weaving," *Transportation Research Part C: Emerging Technologies*, vol. 13, no. 1, pp. 37–62, 2005.

[7] X. Chen, Y. Miao, M. Jin, and Q. Zhang, "Driving decision-making analysis of lane-changing for autonomous vehicle under complex urban environment," in *2017 29th Chinese Control And Decision Conference (CCDC)*. IEEE, 2017, pp. 6878–6883.

[8] S. Moridpour, G. Rose, and M. Sarvi, "Effect of surrounding traffic characteristics on lane changing behavior," *Journal of Transportation Engineering*, vol. 136, no. 11, pp. 973–985, 2010.

[9] B. Zhu, S. Liu, and J. Zhao, "A lane-changing decision-making method for intelligent vehicle based on acceleration field," *SAE International Journal of Passenger Cars-Electronic and Electrical Systems*, vol. 11, no. 2018-01-0599, pp. 219–230, 2018.

[10] C. R. Baker and J. M. Dolan, "Traffic interaction in the urban challenge: Putting boss on its best behavior," in *2008 IEEE/RSJ International Conference on Intelligent Robots and Systems*. IEEE, 2008, pp. 1752–1758.

[11] P. G. Gipps, "A model for the structure of lane-changing decisions," *Transportation Research Part B: Methodological*, vol. 20, no. 5, pp. 403–414, 1986.

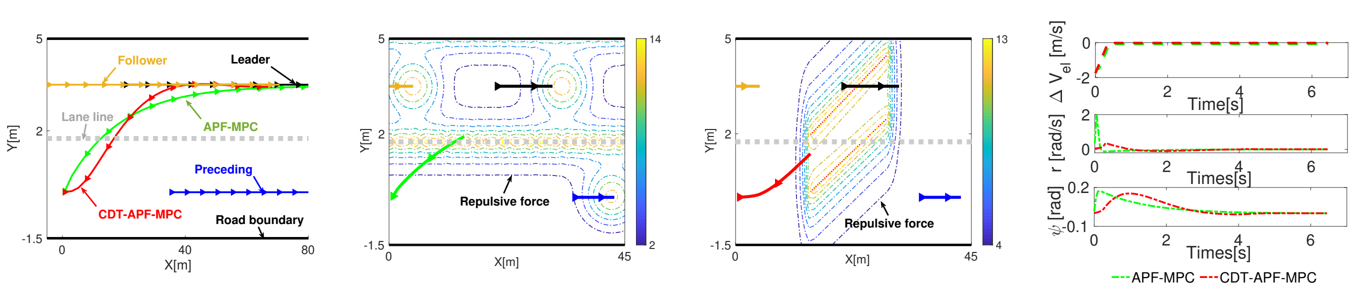

(a) The paths during the lane change maneuvers (b) The repulsive force of the baseline method at $2s$ (c) The repulsive force of the proposed method at $2s$ (d) Vehicle status

Fig. 10: Comparison of motion control results between the proposed and the baseline approaches.

[12] A. Halati, H. Lieu, and S. Walker, “Corsim-corridor traffic simulation model,” in *Traffic Congestion and Traffic Safety in the 21st Century: Challenges, Innovations, and OpportunitiesUrban Transportation Division, ASCE; Highway Division, ASCE; Federal Highway Administration, USDOT; and National Highway Traffic Safety Administration, USDOT.*, 1997.

[13] F. Chen, M. Song, and X. Ma, “Investigation on the injury severity of drivers in rear-end collisions between cars using a random parameters bivariate ordered probit model,” *International journal of environmental research and public health*, vol. 16, no. 14, p. 2632, 2019.

[14] Q. Zeng, H. Wen, H. Huang, and M. Abdel-Aty, “A bayesian spatial random parameters tobit model for analyzing crash rates on roadway segments,” *Accident Analysis & Prevention*, vol. 100, pp. 37–43, 2017.

[15] H. Yu, H. E. Tseng, and R. Langari, “A human-like game theory-based controller for automatic lane changing,” *Transportation Research Part C: Emerging Technologies*, vol. 88, pp. 140–158, 2018.

[16] S. Aradi, “Survey of deep reinforcement learning for motion planning of autonomous vehicles,” *arXiv preprint arXiv:2001.11231*, 2020.

[17] X. Gu, Y. Han, and J. Yu, “A novel lane-changing decision model for autonomous vehicles based on deep autoencoder network and xgboost,” *IEEE Access*, vol. 8, pp. 9846–9863, 2020.

[18] J. Yoo and R. Langari, “A stackelberg game theoretic model of lane-merging,” *arXiv preprint arXiv:2003.09786*, 2020.

[19] G. Li, F. Zhu, X. Qu, B. Cheng, S. Li, and P. Green, “Driving style classification based on driving operational pictures,” *IEEE Access*, vol. 7, pp. 90 180–90 189, 2019.

[20] D. Dörr, D. Grabengiesser, and F. Gauterin, “Online driving style recognition using fuzzy logic,” in *17th international IEEE conference on intelligent transportation systems (ITSC)*. IEEE, 2014, pp. 1021–1026.

[21] F. Göngör and Ö. Tutsoy, “Design and implementation of a facial character analysis algorithm for humanoid robots,” *Robotica*, vol. 37, no. 11, pp. 1850–1866, 2019.

[22] ——, “Design of a chair recognition algorithm and implementation to a humanoid robot.”

[23] S. Yang, W. Wang, C. Lu, J. Gong, and J. Xi, “A time-efficient approach for decision-making style recognition in lane-changing behavior,” *IEEE Transactions on Human-Machine Systems*, vol. 49, no. 6, pp. 579–588, 2019.

[24] W. He, T. Meng, S. Zhang, Q. Ge, and C. Sun, “Trajectory tracking control for the flexible wings of a micro aerial vehicle,” *IEEE Transactions on Systems, Man, and Cybernetics: Systems*, vol. 48, no. 12, pp. 2431–2441, 2018.

[25] T.-T. Tran, S. S. Ge, and W. He, “Adaptive control of a quadrotor aerial vehicle with input constraints and uncertain parameters,” *International Journal of Control*, vol. 91, no. 5, pp. 1140–1160, 2018.

[26] D. Swaroop and S. M. Yoon, “Integrated lateral and longitudinal vehicle control for an emergency lane change manoeuvre design,” *International journal of vehicle design*, vol. 21, no. 2-3, pp. 161–174, 1999.

[27] D. Yang, D. Li, and H. Sun, “2d dubins path in environments with obstacle,” *Mathematical Problems in Engineering*, vol. 2013, 2013.

[28] X. Zhang, A. Liniger, A. Sakai, and F. Borrelli, “Autonomous parking using optimization-based collision avoidance,” in *2018 IEEE Conference on Decision and Control (CDC)*. IEEE, 2018, pp. 4327–4332.

[29] D. Fassbender, A. Mueller, and H.-J. Wuensche, “Trajectory planning for car-like robots in unknown, unstructured environments,” in *2014 IEEE/RSJ International Conference on Intelligent Robots and Systems*. IEEE, 2014, pp. 3630–3635.

[30] O. Khatib, “Real-time obstacle avoidance for manipulators and mobile robots,” in *Autonomous robot vehicles*. Springer, 1986, pp. 396–404.

[31] W. Wang, J. Xi, and D. Zhao, “Learning and inferring a driver’s braking action in car-following scenarios,” *IEEE Transactions on Vehicular Technology*, vol. 67, no. 5, pp. 3887–3899, 2018.

[32] E. J. Chang, O. K. Hussain, and T. S. Dillon, “Application of fuzzy inference systems in real world scenarios,” in *On Fuzziness*. Springer, 2013, pp. 101–107.

[33] T. Toledo, H. N. Koutsopoulos, and M. E. Ben-Akiva, “Modeling integrated lane-changing behavior,” *Transportation Research Record*, vol. 1857, no. 1, pp. 30–38, 2003.

[34] C. Huang, C. Lv, F. Naghdy, and H. Du, “Reference-free approach for mitigating human–machine conflicts in shared control of automated vehicles,” *IET Control Theory & Applications*, vol. 14, no. 18, pp. 2752–2763, 2020.

[35] Z. Zuo, X. Yang, Z. Zhang, and Y. Wang, “Lane-associated mpc path planning for autonomous vehicles,” in *2019 Chinese Control Conference (CCC)*. IEEE, 2019, pp. 6627–6632.

Chao Huang received the Ph.D. degree from the University of Wollongong, Wollongong, NSW, Australia, in 2018. She is currently a Research Fellow with the School of Mechanical and Aerospace Engineering, Nanyang Technological University. Her current research interests include human-machine shared control, path planning of autonomous vehicle.

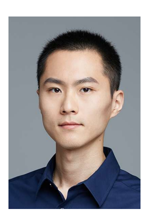

Chen Lv is currently an assistant professor at Nanyang Technology University, Singapore. He received a Ph.D. degree at the Department of Automotive Engineering, Tsinghua University, China in 2016. His research focuses on advanced vehicle control and intelligence, where he has contributed over 90 papers and obtained 12 granted patents.

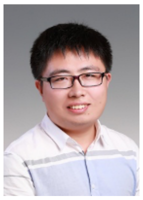

Peng Hang received the Ph.D. degree with the School of Automotive Studies, Tongji University, Shanghai, China, in 2019. He is a Research Fellow with the School of Mechanical and Aerospace Engineering, Nanyang Technological University, Singapore. His research interests include vehicle dynamics and control, decision making and motion control of autonomous vehicles.

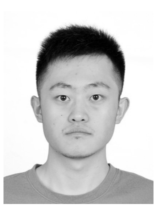

Yang Xing received his Ph. D. degree from Cranfield University, UK, in 2018. He is currently a Research Fellow with the Department of Mechanical and Aerospace Engineering at Nanyang Technological University, Singapore. His research interests include machine learning, driver behavior modeling, and intelligent vehicles.